PHILOSOPHICAL TRANSACTIONS OF THE ROYAL SOCIETY A MATHEMATICAL, PHYSICAL & ENGINEERING SCIENCES

Rydberg series of BaF: peturbation–facilitated studies of core–non–penetrating states

Zygmunt J. Jakubek and Robert W. Field

Phil. Trans. R. Soc. Lond. A 1997 **355**, 1507-1526
doi: 10.1098/rsta.1997.0073

Rydberg series of BaF: perturbation-facilitated studies of core-non-penetrating states

By Zygmunt J. Jakubek† and Robert W. Field

Department of Chemistry, Massachusetts Institute of Technology, Cambridge, MA 02139, USA

Core-non-penetrating molecular Rydberg states sample the electronic structure of the ion core in a uniquely simple way. However, radial overlap and orbital angular momentum propensity rules ($\Delta\ell = \pm 1$) can severely restrict spectroscopic access to $\ell > 3$ non-penetrating states, even via two-colour two-step excitation schemes. Owing to the profoundly different ℓ-uncoupling behaviour of moderate-n^* ($n^* \approx 6$–15) core-penetrating versus non-penetrating states, numerous and systematically repeated perturbations of the Hund's case (b) core-penetrating states (*accidentally* located near integer n^*) by the case (d) non-penetrating states (*always* located near integer n^*) can provide a valuable window into these information-rich, yet difficult to observe, core-non-penetrating states. We report analysis of core-penetrating ($\ell \leqslant 3$)–core-non-penetrating ($\ell > 3$) perturbations in the fluorescence detected optical–optical double resonance spectrum of BaF. One of the perturbers of the $0.86\,^2\Phi$ series is assigned as the lowest energy component, $\mathcal{L} = +5$, of an h complex ($\ell = 5$). Other core-non-penetrating perturbers are assigned as components of g and h complexes. A critical aspect of the assignments of these quite weak and fragmentary interactions between *one* core-penetrating 'bright' state and *many* core-non-penetrating 'dark' states is the systematic (n^* scaling of both matrix element and N values of the level crossing) repetition of each family of perturbations in each successive n^* complex.

1. Introduction

A Rydberg electron can be a sensitive probe of the electronic structure of the ion core. This ion-core structure is sampled in quite different ways by core-penetrating ($\ell \leqslant 3$)–core-non-penetrating ($\ell > 3$) Rydberg series.

The strongest electron↔ion-core interactions occur when the electron is inside the ion core. Information about intra-core energy and angular momentum exchange is encoded in the n^*-invariant shape (apart from the well-known $n^{*-3/2}$ amplitude scaling) of the inner lobes of each core-penetrating series (Mulliken 1964) (n^* is the effective principal quantum number). Therefore, *the primary goal of spectroscopic study or quantum chemical calculations on core-penetrating Rydberg states should be characterization of the shapes of these inner lobes*. These n^*-descaled inner lobes can

† Present address: Inorganic Chemical Physics Laboratory, RIKEN, 2-1, Hirosawa, Wako, Saitama, Japan.

Phil. Trans. R. Soc. Lond. A (1997) **355**, 1507–1526
Printed in Great Britain

be represented by

$$\psi_{r\ell'\lambda} \sim \sum_{\ell} a_\ell Y_{\ell\lambda}(\theta,\phi) R_\ell(r),$$

where the partial-ℓ characters, a_ℓ, and the shape of each ℓ-dependent radial factor are somehow to be determined by experiment or calculation. Perhaps the most sensitive experimental probe of these partial-ℓ characters and radial shapes for the common intra-core lobe of all members of each core-penetrating Rydberg series is obtained from the low-n^* deviations of molecular constants from their asymptotic values as the series is followed to its lowest-n^* valence terminus state (Berg *et al.* 1993). (The 'asymptotic' values are most easily obtained in the $n^* \approx 5$–10 region, before the higher-n^* onset of profound ℓ-uncoupling effects at low N, due to off-diagonal $B\boldsymbol{N}\cdot\boldsymbol{l}$ matrix elements, which require a laborious supercomplex deperturbation fitting procedure.)

The compact nature ($r \lesssim 1$ Å) of these information-rich inner lobes makes them an ideal target for quantum chemical calculations. The usual disclaimer, that quantum chemical calculations are ill suited for the diffuse orbitals, which are an essential feature of all Rydberg states, does not apply! A great opportunity for insight and quantitative predictions exists if the results of high level wavefunction calculations on the inner lobes of low-n^* core-penetrating Rydberg states could be embedded into an n^*-scaled multichannel model. It is also possible to obtain a satisfactory atomic-ion in-molecule semi-empirical description of the intra-core e^-–ion interaction from a ligand field (Rice *et al.* 1985) or a multiple scattering model (Harris & Jungen 1993). Since this paper will focus on core-non-penetrating states, the preceding provocative remarks about the most intensely studied class of Rydberg states, the core-penetrating series, will have to suffice.

Although the electron↔ion-core interactions for core-non-penetrating Rydberg series are much weaker than those for core-penetrating series (Jungen & Miescher 1969; Eyler & Pipkin 1986; Watson 1994), it can be argued that they are considerably more important in describing the exchange of energy and angular momentum between the electron and ion core. Their importance arises from their vastly greater abundance (there are, respectively, only six s∼p∼d and ten s∼p∼d∼f, core-penetrating $^2\Lambda$ series in CaF (Murphy *et al.* 1990) and BaF (Jakubek & Field 1994), whereas the number of non-penetrating $^2\Lambda$ series, $(n+1)(\frac{1}{2}n)-6$ or 10, increases rapidly with n). Since, in non-penetrating states, the Rydberg electron does not penetrate inside the ion core, the small shifts of non-penetrating series from integer values of n^* sample the multipole moments and polarizabilities (and the internuclear distance dependence of these quantities) of the ion core (Jungen & Miescher 1969; Eyler & Pipkin 1986; Watson 1994; Sturrus *et al.* 1988; Dill & Jungen 1980; Ross 1991). Although core-penetrating Rydberg series also sample these long-range multipolar properties, the spectroscopic structure of core-penetrating series is dominated by short-range intra-core interactions. Ideally, the multipole quantities should be determined first from an analysis of non-penetrating series (or from high level quantum chemical calculations of the ion-core multipole moments) *before* a definitive analysis of the core-penetrating series is undertaken.

Despite their importance, and the fact that they exist for all molecules, core-non-penetrating Rydberg series have received very little experimental (Herzberg & Jungen 1982; Dressler *et al.* 1981; Fujii & Morita 1995) or theoretical attention. One reason for this neglect is that core-non-penetrating Rydberg series are often extremely difficult to observe and even more difficult to interpret. In this paper we

Table 1.

ℓ	2^ℓ moment (AU)	
1	dipole	−4.41
2	quadrupole	−11.48
3	octupole	−41.45
4	hexadecapole	−142.35

will illustrate both the difficulties of observation and assignment as well as a new, n^*-scaling based, method for uncovering a few diagnostically important members of these ubiquitous but shy non-penetrating series.

A long-range model for non-penetrating molecular Rydberg series was first proposed by Jungen & Miescher (1969). They were able to describe the 4f and 5f complexes of NO to experimental precision using only four adjustable parameters: (i) the ion-core quadrupole moment; (ii) an isotropic and (iii) an anisotropic polarizability; and (iv) the NO^+ rotational constant, B^+. The long-range multipolar core model (Jungen & Miescher 1969; Eyler & Pipkin 1986; Watson 1994) has been applied to several other molecules (CO (Komatsu *et al.* 1995), H_2 (Eyler & Pipkin 1986; Sturrus *et al.* 1988; Herzberg & Jungen 1982), N_2 (Huber *et al.* 1994; McCormack *et al.* 1990), NO (Dressler *et al.* 1981; Fujii & Morita 1995) etc.).

Our studies of the Rydberg states of the alkaline earth monohalides (CaF (Berg *et al.* 1993; Murphy *et al.* 1990, 1995; Harris & Field 1993; Gittins *et al.* 1993; Jakubek *et al.* 1994), CaCl (Li *et al.* 1998) and BaF (Jakubek & Field 1994, 1996, 1998; Jakubek *et al.* 1994)) introduce new challenges. These molecules are extremely polar and relatively heavy ($B^+ < 0.35\ \mathrm{cm}^{-1}$). Not only are the even multipole moments of the molecular ion core considerably larger than those of all previously well studied (near homonuclear) molecules, but the odd multipole moments are enormous. The magnitudes of the multipole moments are so large that all perturbation theoretic relationships (Jungen & Miescher 1969; Eyler & Pipkin 1986; Watson 1994) between the multipole moments and the observable ℓ, λ splittings and $\Delta\ell \neq 0$, $\Delta\lambda = 0$ interactions are invalidated (Watson 1994). The BaF^+ multipole moments, naively estimated using a Ba^{2+}, F^- two point charge model (ignoring both atomic-ion polarizabilities and orbital overlap effects) are listed in table 1 (calculated as $Z_+ r_+^\ell + Z_- r_-^\ell$, where $Z_+ = +2$ and $Z_- = -1$, r_+ is the (negative) distance of M^{2+} from the centre of mass and r_- is the (positive) distance of X^- from the centre of mass, with the coordinate origin at the centre of mass, $R_e^+ = 3.93$ AU). The actual values of the multipole moments will be slightly smaller, owing primarily to the dipole on F^- induced by Ba^{2+} (Field & Gittins 1997).

2. Experiment

Our experiments on the Rydberg states of BaF have been described previously (Jakubek & Field 1994, 1996, 1998). A brief description is presented subsequently. Most of the results discussed in this paper are obtained in a *fluorescence-detected* optical–optical double resonance (OODR) experiment in which the $v = 0$ $C^2\Pi_{3/2}$ state was used as the intermediate level. However, some results from mass-selected, *ion-detected*, OODR experiments, again using the $v = 0$ $C^2\Pi_{3/2}$ state as the inter-

mediate level, are also discussed below. Details of the ion-detected experiments will be presented elsewhere (Ma *et al.*, unpublished work).

Barium monofluoride molecules are produced in a high temperature oven by resistive heating of BaF_2 powder with a small amount of boron powder. The BaF_2 and B are contained in a graphite crucible which is supported in, and heated by, a tungsten basket. A single load of BaF_2 (*ca.* 30 g) is sufficient for about 6–8 h of operation. The oven is slowly (*ca.* 30–40 min) heated and, during normal operation, the power input to the tungsten basket heater does not exceed 255 W (4.4 V, 58 A, 60 Hz AC). The maximum power is applied only when the highest-n^* ($n^* \approx 13$–14) states are studied. Flowing argon, at a pressure of about 200 mTorr, carries BaF molecules out of the oven region and into the excitation region. The BaF molecules are cooled rotationally and vibrationally to approximately 500 K.

The PUMP laser (Spectra Physics, PDL-1) selectively populates an individual rotational level of the $v = 0$ $C^2\Pi_{3/2}$ state. As the PROBE laser (Lambda Physik, FL3002E) is scanned, an OODR spectrum is recorded by detecting both direct and cascade fluorescence from Rydberg states down to the $X^2\Sigma^+$ ground state. Both dye lasers are pumped by the second or third harmonic of the same Nd:YAG laser (Quanta Ray, DCR-2A, 10 Hz) and usually operated with intra-cavity etalons (PUMP laser bandwidth less than 0.05 cm^{-1}, PROBE laser bandwidth less than 0.03 cm^{-1}). The laser pulse energy is kept low enough to avoid power broadening the spectra. For the highest ($n^* \approx 14$) observed Rydberg states, the PROBE laser energy does not exceed 500 μJ $pulse^{-1}$ and is much lower for low- and intermediate-n^* Rydberg states. Both PUMP and PROBE laser beams are expanded and their effective diameter in the excitation region is limited to 2.5 cm by the input window.

Fluorescence from the intermediate state is detected by a photomultiplier tube (Hamamatsu, R928) equipped with a narrow band (5 nm) interference filter centred at 500 nm. UV fluorescence from Rydberg states is detected by a solar blind photomultiplier tube, PMT (Hamamatsu, R166) through a solar blind broadband interference filter (Oriel), centred at 290 nm (65% peak transmission). The signal from the PMT is gated and integrated by a dual channel boxcar (Stanford Research Systems, SR250) and recorded by a computer. The opening of the gate coincides with the arrival of the PROBE laser pulse (no delay) and typical gate widths are 100–500 ns. Simultaneously with the Rydberg spectrum, an I_2 fluorescence excitation spectrum is recorded, using a portion of the PROBE beam, for absolute frequency calibration (0.01–0.02 cm^{-1}) (Gerstenkorn & Luc 1979). The signal and reference channels are usually averaged over 5–10 laser shots per point. Low resolution scans are carried out with a step size of $\Delta\lambda = 0.002$ nm (0.06 cm^{-1}). In high resolution scans, various step sizes in the range of $\Delta\nu = 0.008$–0.012 cm^{-1} are used.

3. Observations of core-non-penetrating Rydberg states

(*a*) *Intermediate state* $C\,^2\Pi$

The $C\,^2\Pi$ state, $T_0 \approx 20\,086$ cm^{-1}, is conveniently located approximately halfway between the $X\,^2\Sigma^+$ ground state and the ionization limit, IP = 38 745 cm^{-1}. It is therefore used as an intermediate level not only in the OODR scans presented here, but also in other double-resonance experiments on the Rydberg states of BaF. The PUMP electronic transition, $C\,^2\Pi_{3/2}$–$X\,^2\Sigma^+$ (Effantin *et al.* 1990), is extremely congested due to the similarity of rotational and vibrational constants in the upper and lower electronic states as well as a very rich isotope structure (five isotopic

species of Ba are observable). Therefore, by pumping in the $C_{3/2}$–$X(0,0)$ band, we are only able to access $J = 6.5$ (via the $R_{2f}(5.5)$ line) as the lowest rotational level of f symmetry and $J = 14.5$ (via the ${}^{S}R_{21ef}(13.5)$ line) as the lowest rotational level of e symmetry. Lower J lines are obscured by very congested bandheads. This poses severe problems of assignment. In order to conclusively assign our double resonance spectra, it is necessary to record spectra for several consecutive J levels, in some cases spectra for every J up to $J = 20.5$ for both e and f symmetries! Ultimately, however, this inconvenient necessity becomes an invaluable advantage, because it allows us to pick out multiple low J core-penetrating and core-non-penetrating perturbations and in this way, assemble a large and relatively comprehensive data set for core-non-penetrating Rydberg states. These observations of the non-penetrating states are the most exciting, although serendipitous, results of our series of experiments on the BaF Rydberg states.

(*b*) *Core-penetrating–core-non-penetrating perturbations*

The electronic structure of the BaF molecule possesses an interesting feature: six of the ten series of core-penetrating ${}^2\Lambda$ states are clustered near integer n^*. We know *a priori* that *all* core-non-penetrating states must be even more strongly clustered near integer n^*. The ℓ-uncoupling effects (due to matrix elements of $B\boldsymbol{l}\cdot\boldsymbol{N}$ off diagonal in Λ (Lefebvre-Brion & Field 1986)) for the core-non-penetrating states are expected to be much stronger than for the core-penetrating states because of the small energy separations (relative to the $\Delta\ell = 0$, $\Delta\Lambda \neq 0$ off-diagonal matrix elements of $B^+\boldsymbol{l}_\pm\boldsymbol{N}_\mp$) between the rotationless Λ states in the non-penetrating complexes. This ℓ uncoupling causes the effective rotational constants for the top and bottom energy components of each non-penetrating $n\ell$ complex to be respectively much larger and smaller than B^+. In contrast, the effective rotational constants for the core-penetrating states are much less affected by ℓ uncoupling (smaller matrix elements, larger energy differences) and are clustered near B^+. Such a situation inevitably leads to multiple avoided crossings between core-non-penetrating and core-penetrating states. Near each avoided crossing (a few J values), the core-non-penetrating states borrow some core-penetrating character, and this makes their excitation via the $C^2\Pi$ state and detection via cascade fluorescence possible.

We observe multiple core-penetrating–core-non-penetrating perturbations. The easiest to detect are the strong perturbations in the 0.86 ${}^2\Phi$ and 0.94 ${}^2\Delta$ series. More difficult to identify is a series of very weak perturbations in the 0.88 ${}^2\Sigma^+$ series. We also observe an extra state (manifest as complete rotational term curve) in the region just above integer n^*. Conclusive assignments of the core-non-penetrating perturbers in the n^* slightly larger than integer region are not yet possible and more experiments are required.

The systematic perturbations in the 0.94 ${}^2\Delta$ series are observed for the 8.94 ${}^2\Delta$ state and higher series members. In figures 1 and 2, three perturbations are evident in the 10.94 ${}^2\Delta$ state, two of them, one strong and one very weak, in the 10.94 ${}^2\Delta^+$ (open triangles) component and one (weak) in the 10.94 ${}^2\Delta^-$ component (solid circles). For the 10.86 ${}^2\Phi$ state we observe one strong perturbation and the onset of another at high N in the 10.86 ${}^2\Phi^+$ component (open triangles) and one or two very weak perturbations in the 10.86 ${}^2\Phi^-$ component (solid circles). As we go to higher n^* members of the ${}^2\Phi$ series (figure 3), additional perturbations are observed at high N. The perturbation in the 0.88 ${}^2\Sigma^+$ series is very weak and not very well documented. In the 10.88 ${}^2\Sigma^+$ state (figures 1 and 2) only six extra lines are detected

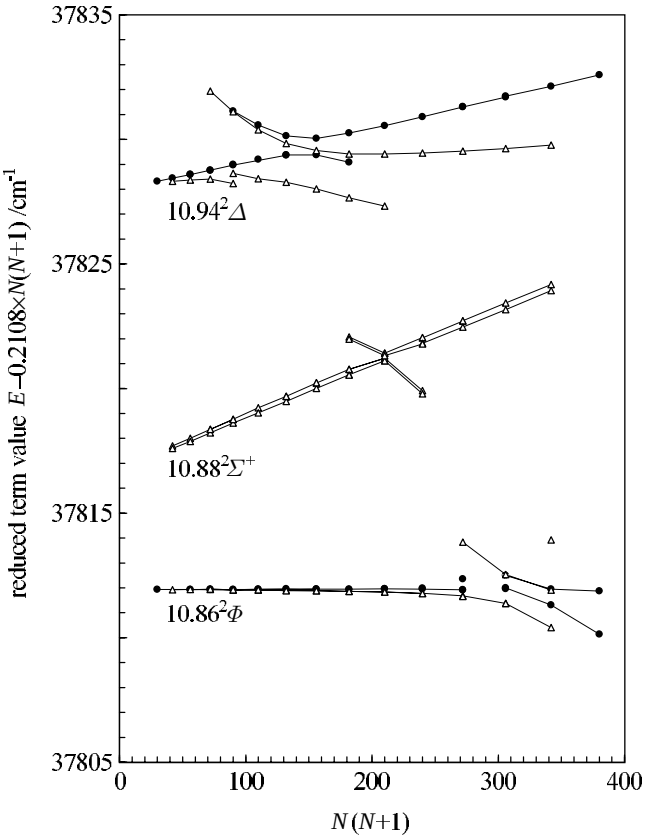

Figure 1. Plot of reduced term values versus $N(N+1)$ for the $v^+ = 0$ 10.86 $^2\Phi$, 10.88 $^2\Sigma^+$ and 10.94 $^2\Delta$ states, showing multiple perturbations by core-non-penetrating states. Open triangles (solid circles) denote levels of $+(-)$ Kronig symmetry. Note how, on this 'N plot', the spin splitting of the core-penetrating states almost disappears. This illustrates that N, not J, is the pattern-forming quantum number for case (b) states. All of the spin-doubled core-penetrating states appear to be perturbed from above by a non-spin-doubled component of a core-non-penetrating state.

and the largest level shift is approximately 0.1 cm^{-1}. Figure 1 is a plot of reduced term value versus $N(N+1)$. To better illustrate the core-penetrating–core-non-penetrating perturbations, we also present in figure 2 the reduced term value plot versus $J(J+1)$ for e-symmetry levels. Recall that J, unlike N, is a rigorously good quantum number. Also the total Hamiltonian is strictly block diagonal for e- versus f-symmetry levels.

Figures 1 and 2 also illustrate an important point about the rotational and fine structure of core-penetrating states. When the reduced term values of an isolated case (b) state are plotted versus $N(N+1)$ as in figure 1, the two spin components of a $\Lambda \neq 0$ $^2\Lambda$ state fall nearly on top of each other. The remaining (small) separation between same-N, same-parity $J = N + \frac{1}{2}$ states is primarily a pseudo spin-rotation splitting, which is due to the approximately n^*-invariant effects of $\Delta\Lambda \neq 0$ spin–orbit interactions (second-order $\boldsymbol{H}^{\mathrm{spin-orbit}} \times \boldsymbol{H}^{\mathrm{rotation}}$). When plotted versus $J(J+1)$ as in figure 2, this spin splitting appears much larger and much more strongly J dependent. The two components of a case (b) $^2\Lambda$ state are much easier to recognize

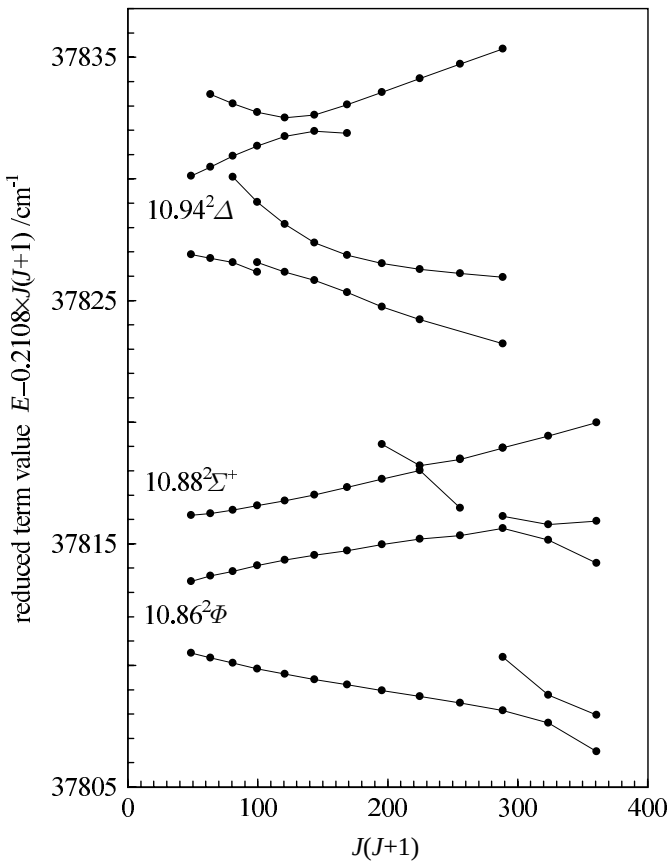

Figure 2. Plot of reduced term values versus $J(J+1)$ for the e levels of the $v^+ = 0$ 10.94 $^2\Delta$, 10.88 $^2\Sigma^+$, and 10.86 $^2\Phi$ states, illustrating core-penetrating–core-non-penetrating perturbations. This 'J plot' contains the same e-parity data as shown on figure 1. Although the larger splitting between spin components makes it more difficult to recognize the two halves of the $^2\Delta$ and $^2\Phi$ states, the plot versus $J(J+1)$ makes it easier to see which pairs of term curves perturb each other. Note that the e-symmetry part of the $^2\Sigma^+$ state appears here as a single term curve perturbed once (weakly) from above. The term curve just below the 10.88 $^2\Sigma^+$ state is the upper (F_2) spin component of the 10.86 $^2\Phi$ state.

on an N plot (figure 1) than a J plot (figure 2), but effects (level shifts, extra lines) of local perturbations that always occur at $\Delta J = 0$ intersections of rotational term curves, are much easier to understand on a J plot. As will be seen later, core-non-penetrating states follow case (d) and the $2\ell + 1$ components of an ℓ complex are so widely separated on an N plot that they appear as separate states.

The appearance of the reduced term value plots, as we follow the three Rydberg series, is very similar. Corresponding perturbations appear at high N for low-n^* states and move systematically towards lower N as n^* increases (figures 3 and 4). This systematic shift of all penetrating–non-penetrating perturbations to lower N as n^* increases, reflects the n^{*-3} scaling of the energy difference between the core-penetrating (non-integer n^*) and the hydrogenic (integer n^*) non-penetrating state. The $\Delta J = 0$, $\Delta N = 0$ energy separations between different core-penetrating electronic states is much larger than the $B\boldsymbol{l}_{\pm}\boldsymbol{N}_{\mp}$ interaction matrix elements (Hund's case (a) or (b)) (Lefebvre-Brion & Field 1986), thus the ℓ-uncoupling interactions

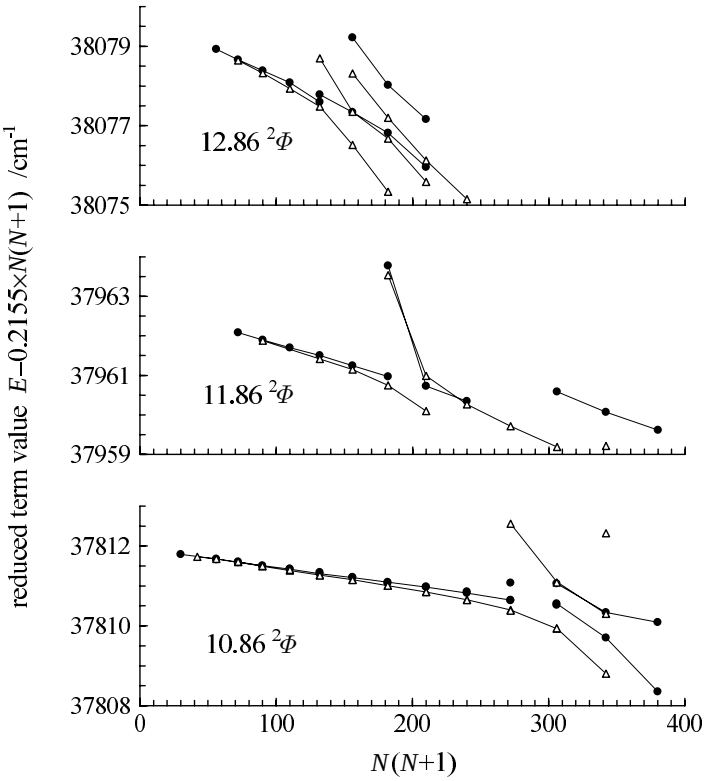

Figure 3. Systematic shifts of replicated perturbations in the $v^+ = 0$ 0.86 $^2\Phi$ series as n^* increases (Φ^+ open circles, Φ^- filled circles.) The bottom panel shows the same state as shown in figure 1. The key points to notice are that, as n^* increases, the lowest-N perturbation shifts systematically to lower N, and, just above the lowest-N perturber there are many other downward moving, closely spaced perturbers. It becomes very difficult to disentangle the successive perturbers.

among those states can be neglected. The effective rotational constants of penetrating states do not change significantly with n^* in the $6 \leqslant n^* \leqslant 14$ region. In contrast, the core-non-penetrating states are described well by Hund's case (d) (Lefebvre-Brion & Field 1986). For these states the ℓ-uncoupling $B^+\boldsymbol{l}_\pm\boldsymbol{N}_\mp$ rotational interaction is large relative to the electronic separations between rotationless Λ states. The effective rotational constants for the low energy components of the non-penetrating complexes are very small (relative to B^+) and do not change (significantly) with n^*. In effect, for increasing consecutive-n^* members of a core-penetrating Rydberg series, the crossings between core-penetrating and core-non-penetrating terms occur at lower and lower J. Eventually, as n^* increases, multiple level crossings appear simultaneously even at very low J. In addition, the ℓ-uncoupling interactions among the core-penetrating states become important at progressively lower J values and the low J effective B values of the core-penetrating states become strongly n^* dependent. Eventually, at $n^* \approx 14$, this picture of isolated perturbations moving systematically to lower J values breaks down. The window for detecting and exploiting these isolated repeated systematically J-scaling core-penetrating–non-penetrating perturbations extends from $6 \lesssim n^* \lesssim 14$ for BaF.

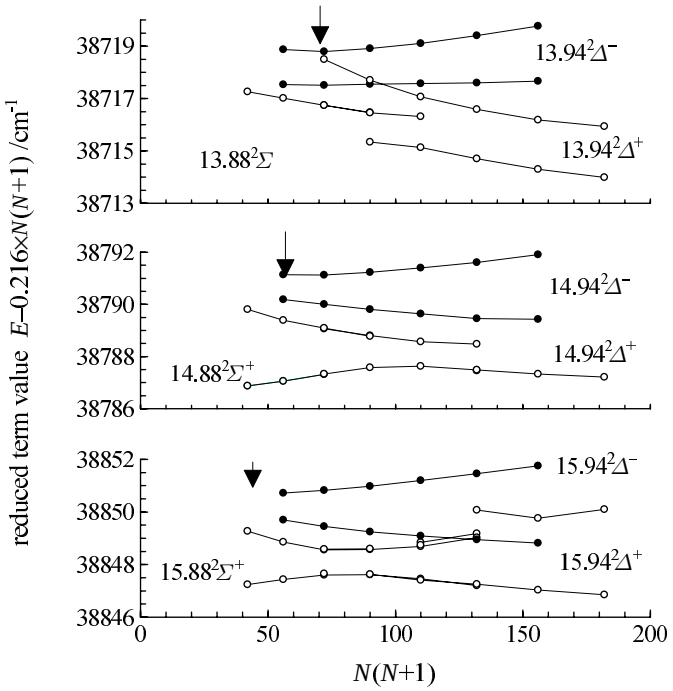

Figure 4. Systematic shifts of replicated perturbations in the $v^+ = 1\ 0.94^2\Delta$ and $v^+ = 1\ 0.88\ ^2\Sigma^+$ series as n^* increases. (+(−)Kronig symmetry open (filled) circles.) Two kinds of perturbations appear. The 0.88 $^2\Sigma^+$ state crosses through 0.94 $^2\Delta^+$ from below. This perturbation between core-penetrating states also shifts systematically to lower N as n^* increases. Non-penetrating states cross through $^2\Delta$ from above, intersecting $^2\Delta^+$ at higher N than $^2\Delta^-$. The arrows mark the location of the lowest-N crossing in the $^2\Delta^-$ state.

(*c*) *Perturbations in the 0.86* $^2\Phi$ *series*

The repeated perturbations in the 0.86 $^2\Phi$ series hold the key to the ℓ assignments of the core-non-penetrating states. *A priori*, all one knows is that $(n+1)(\frac{1}{2}n)$–10 non-penetrating $^2\Lambda$ states of BaF live near integer n^* (i.e. at $n = 10$ there are 45 different non-penetrating $^2\Lambda$ states, belonging to $4 \leqslant \ell \leqslant 9$). Some sort of simplified model is needed to predict the following.

(i) Which of the non-penetrating states will cross through (from above) a penetrating state situated $1.00 - 0.86 = 0.14$ below integer n^*?

(ii) As J increases, what is the order in which the ℓ, Λ (case b) or $\ell, \mathcal{L}$ (case d) non-penetrating states cross through the 0.86 penetrating state?

(iii) What is the slope of the reduced rotational term value curve for each $\ell, \mathcal{L}$ non-penetrating state at the J value of its ($\Delta J = \Delta N = 0$) intersection with the 0.86 penetrating state?

(iv) What is the perturbation matrix element at this level crossing? Is the matrix element large enough to guarantee detection or small enough to be undetectable (at the resolution, precision, and dynamic range of the specific experiment)? In between the limits of *guaranteed* detection or non-detection, there is the *possibility* of detection if a near perfect coincidence of interacting zero-order energy levels occurs, and the multiple possibilities of such a coincidence occurring at one of several successive n^* values.

The first step is to calculate the nonrotating n^* values of all ℓ, Λ-non-penetrating

Table 2.

	$^2\Sigma^+$	$^2\Pi$	$^2\Delta$	$^2\Phi$	$^2\Gamma$	^{2}H	CG
$11g$	11.0934	11.0738	11.0256	10.9589	10.8807	—	10.9968
$11h$	11.0487	11.0432	11.0273	11.0021	10.9690	10.9296	10.9992
Δn	0.0447	0.0306	−0.0017	−0.0432	−0.0883	—	

states. Using a multipole-core model (prolate spheroidal coordinates) and multipole moments computed from the naive $+2, -1$ point charge distribution we get table 2.

The spread in n^* values is slightly larger than that which would be expected for a realistic model in which Ba^{2+} and F^- atomic-ion polarization effects reduce the molecular-ion-core multipole moments. It is clear that *all* the non-rotating non-penetrating ℓ, Λ states are higher lying than the 0.86 $^2\Phi$ state. The range of n^* values spanned by the Λ components of each ℓ complex decreases rapidly with ℓ (therefore the splittings of the $\ell = 6, 7, 8, 9$ complexes are not shown). Similarly, the offset from integer n^* of the centre of gravity (CG) of each ℓ complex decreases rapidly with ℓ. Finally, since ℓ mixing, induced by the core multipole moments, follows a $\Delta\Lambda = 0$ selection rule, the most severe ℓ mixing (at low N^+) is expected for the middle components of each ℓ complex because these components have the smallest $\Delta\Lambda = 0$ energy separations (shown as Δn in table 2).

It appears that, as N increases, the 0.86 $^2\Phi$ state will eventually cross and thus be perturbed by *all* of the components of *all* non-penetrating ℓ complexes for which the B_{eff} value is smaller than B^+. In order to expose the diagnostic features of each ℓ, Λ or $\ell, \mathcal{L}$ substate, that will become its perturbation signature when imposed via perturbation on the 0.86 $^2\Phi$ state, it is necessary to examine the rotational behaviour of a case (d) complex (Lefebvre-Brion & Field 1986). In the case (d) limit, the pattern-forming rotational quantum number is N^+ and, for all $2\ell + 1$ components of an ℓ complex,

$$T^{(\mathrm{d})}(N^+) = B^+ N^+(N^+ + 1). \tag{3.1}$$

Each N^+ level has $2\ell + 1$ N components (or $2N + 1$ when $N < \ell$), where

$$\boldsymbol{N} \equiv \boldsymbol{N}^+ + \boldsymbol{l}, \tag{3.2}$$

$$N - N^+ \equiv \mathcal{L} \quad \text{and} \quad \mathcal{L} = -\ell, -\ell + 1, \ldots, +\ell. \tag{3.3}$$

$\mathcal{L}$ is the projection of $\boldsymbol{l}$ along the direction of $\boldsymbol{N}$. Since the core-penetrating states follow the case (b) pattern, where N rather than N^+ is the pattern-forming rotational quantum number,

$$T^{(\mathrm{b})}(N) = B^+ N(N + 1), \tag{3.4}$$

it will be useful to re-express $T^{(\mathrm{d})}$ in terms of N and $\mathcal{L}$ rather than N^+

$$T^{(\mathrm{d})}(N, \mathcal{L}) = B^+(N - \mathcal{L})(N - \mathcal{L} + 1) \tag{3.5}$$

$$= B^+ N(N + 1) + B^+ \mathcal{L}(\mathcal{L} - 1) - 2B^+ \mathcal{L} N. \tag{3.6}$$

Thus, if the *reduced rotational term value*,

$$T^{(\mathrm{d})}(N, \mathcal{L}) - B^+ N(N + 1), \tag{3.7}$$

is plotted versus N, a straight line will be obtained with slope $-2B^+\mathcal{L}$ (and intercept

$E_{CG} + B^+\mathcal{L}(\mathcal{L}-1)$). Since B^+ is usually known from the previous analysis of many isolated core-penetrating series, the slope of this reduced term value plot determines $\mathcal{L}$ for an unknown perturber, provided that at least two consecutive rotational term values of this non-penetrating perturber can be observed. Note that the slopes and intercepts do not depend on ℓ. Thus the case (d) term curves for all non-penetrating ℓ occur as parallel groups within each common $\mathcal{L}$ value, and the energy order of ℓ components at each N, within each $\mathcal{L}$ group, is determined by the predicted energy order of the non-rotating centres of gravity of the ℓ complexes. This means that, as a penetrating state is followed from $N = \Lambda$ toward higher N, the perturbations by non-penetrating states will occur in $\mathcal{L}$ groups, the highest $\mathcal{L}$ first (last) if the penetrating state lies below (above) integer n^*. Within each $\mathcal{L}$ group, the perturbations will occur in order of increasing ℓ. There is also a Kronig symmetry† selection rule, provided that spin–orbit perturbations can be neglected. A core-penetrating level of + Kronig symmetry can only be perturbed by a non-penetrating state of + Kronig symmetry $[(-1)^{\ell+\mathcal{L}}]$.

The last piece of the assignment puzzle, 'what is the highest ℓ-value detectable through perturbations?', is provided by the expectation that the perturbation matrix elements decrease rapidly as ℓ increases (Jungen & Miescher 1969; Eyler & Pipkin 1986; Watson 1994). This means that the highest detectable ℓ value is determined by the maximum $|\mathcal{L}|$ value among all non-penetrating perturbers observed for a given penetrating state. The 0.86 $^2\Phi$ state is ideally situated to provide this upper bound on perturbation-detectable ℓ values because it is a nearly pure f ($\ell = 3$) state.

The 0.86 $^2\Phi$ state is also located not so close to integer n^* that the non-penetrating ℓ complexes are able to undergo nearly complete ℓ uncoupling (transition to case (d)) before the lowest-N perturbation is reached. This confers two benefits:

(i) $\mathcal{L}$-diagnostic slopes are observable on reduced term value plots;

(ii) less restrictive case (b)–(d) than case (b)–(b) selection rules make it possible (in principle) to observe all $\mathcal{L}$ values via perturbations of a single Λ state.

Figures 1 and 2 are reduced term value plots for the 10.86 $^2\Phi$, 10.88 $^2\Sigma^+$, and 10.94 $^2\Delta$ states. The 10.86 $^2\Phi$ state is the key to the $\ell, \mathcal{L}$ assignments of the core-non-penetrating states that emanate from $n^* = 11$. The first (lowest-N) level crossing in the 10.86 $^2\Phi^+$ ('+' means + Kronig symmetry) state appears to occur near $N = 17$ $[N(N+1) = 306]$. The lowest-N perturbation will involve a state with the highest observable $\mathcal{L}$ value and this in turn will suggest the highest ℓ value detectable via perturbations of any of the ten well-known core penetrating $^2\Lambda$ Rydberg series. A careful investigation of the reduced term value plot reveals no other systematic level shifts (larger than our approximately 0.01 cm^{-1} detection threshold) that would suggest an additional, lower-N perturbation. (This is not a blind search. One knows where to look and what to look for. If one were to perform a limited number of higher

† Kronig symmetry is defined by the reflection symmetry of the spatial part of the electronic wavefunction and is related to total ± parity by a factor of $(-1)^N = (-1)^{N^+ + \mathcal{L}}$. What we have described here as 'Kronig symmetry' is identical to the $\Lambda(A')/\Lambda(A'')$ symmetry discussed by Alexander *et al.* (1988). Although for a non-singlet state, the spatial part of the electronic wavefunction has well-defined symmetry with respect to reflection through a plane perpendicular to the nuclear rotation ($\bar{R}$ or $\bar{N}^+$) only in the Hund's case (b) or (d) limit, Alexander *et al.* (1988) show how $\Lambda(A')/\Lambda(A'')$ symmetry may always be rigorously defined. Since we are concerned here primarily with perturbation selection rules for the $B[N-l]^2$ operator (Lefebvre-Brion & Field 1986), the $^{2S+1}\Lambda \neq 0$ states that are connected to a $^{2S+1}\Sigma^+$ state by multiple applications of the BN^+l^- operator have + Kronig symmetry, are symmetric with respect to reflection of the spatial coordinates of the electronic wavefunction through the plane of rotation, and are of $\Lambda(A')$ or Λ_+ symmetry.

resolution higher sensitivity experiments, in search of higher-$\mathcal{L}$ (or higher-ℓ) states, the $N < 17$ region of the BaF 10.86 $^2\Phi$ $v = 0$ state would be optimal.) From the extra lines and level shifts observed at $N = 17$ and 18, we obtain

$$T_{\rm pert}(18) - T_{\rm pert}(17) = 6.03\ {\rm cm}^{-1} \tag{3.8\,a}$$

$$= 2B^+[18 - \mathcal{L}], \tag{3.8\,b}$$

and given that $B^+ \approx 0.234\ {\rm cm}^{-1}$, we obtain

$$\mathcal{L} \approx 5.1.$$

This suggests that the core-non-penetrating perturber is the $\mathcal{L} = 5$ component of the $\ell = 5$ (h) complex. The Kronig symmetry of $\ell = 5$, $\mathcal{L} = 5$ is +, which is consistent with the selection rule for perturbations of a Φ^+ state. $\mathcal{L}$=5 is too high (and the Kronig symmetry is wrong) for $\ell = 4$ (g). The only other plausible ℓ–assignments are $\ell = 7$ (k) and 9 (m), but these would imply the presence of detectable lower–N $\mathcal{L} > 5$ perturbations.

The 10.86 $^2\Phi^-$ state is weakly perturbed twice, at $N = 17$ and also probably at $N = 16$. From the extra lines we calculate $\mathcal{L}_{\rm exp} = 4.3$, thus the likely perturber is $\ell = 5, \mathcal{L} = 4$, a −Kronig symmetry state. The presence of a second perturbation at $N = 16$ $[N(N + 1) = 272]$ is inferred from only one extra line and a very small level shift. That perturbation cannot be corroborated by perturbations in higher-n members of the 0.86 $^2\Phi$ series. Insufficient information is available to determine an $\mathcal{L}$ value, but a plausible assignment for the second non-penetrating perturber is $\ell = 6$, $\mathcal{L} = 5$, − Kronig symmetry.

The 11.86 $^2\Phi$ state exhibits two strong perturbations in the $^2\Phi^+$ component and one strong perturbation (and possibly a second one) in the $^2\Phi^-$ component (see figure 3, middle panel). As expected, these perturbations are shifted to lower N values relative to the corresponding perturbations in the 10.86 $^2\Phi$ state. Specifically, the perturbation at $N = 17$ in 10.86 $^2\Phi^+$ moves to $N = 14$ in 11.86 $^2\Phi^+$ and to $N \approx 12$ in 12.86 $^2\Phi^+$; similarly, the strong perturbation at $N = 18$ in 11.86 $^2\Phi^+$ moves to $N = 14$ in 12.86 $^2\Phi^-$. In addition, the 12.86 $^2\Phi$ state shows two weak perturbations, at $N = 11$ in $^2\Phi^-$ and $N \approx 13$–14 in $^2\Phi^+$.

(*d*) *Perturbations in the 0.88* $^2\Sigma^+$ *series*

Figure 5 shows that the 10.88 $^2\Sigma^+$ state is perturbed from above at $N = 14$ $[N(N + 1) = 210]$. The main perturbation of the 10.88 $^2\Sigma^+$ state is quite weak, the maximum observed shift of the main lines is only approximately 0.06 cm^{-1}. Figures 1, 2 and 5 show that the curvature of the perturber term curve is anomalous. The slope of this term curve becomes increasingly negative as N increases, which is the opposite of what one would expect for an isolated non-penetrating state. One explanation is that the 10.88 $^2\Sigma^+$ state is perturbed by two non-penetrating states which in turn undergo an avoided crossing near the perturbation region. Thus, if we calculate $\mathcal{L}_{\rm exp}$ separately from the $N = 13$–14 and $N = 14$–15 intervals at energies, respectively, above and below the 10.88 $^2\Sigma^+$ state (see figure 5), we obtain $\mathcal{L}_{\rm exp} = 1.8$ and $\mathcal{L}_{\rm exp} = 4.3$. These $\mathcal{L}$ values suggest assignment of the non-penetrating perturbers as $\ell = 5$, $\mathcal{L} = 3$, + and $\ell = 4$, $\mathcal{L} = 4$, + for the $N = 13$–14 and $N = 14$–15 intervals, respectively. Since the $^2\Sigma^+$ state is of + Kronig symmetry, the $\mathcal{L} = 3$ component of the $g(\ell = 4)$ complex and $\mathcal{L} = 4$ component of the $h(\ell = 5)$ complex are excluded as perturbers. Although both $\mathcal{L}_{\rm exp}$ values are distressingly far from integer values, the fact that one is smaller and the other larger than integer supports our suggestion

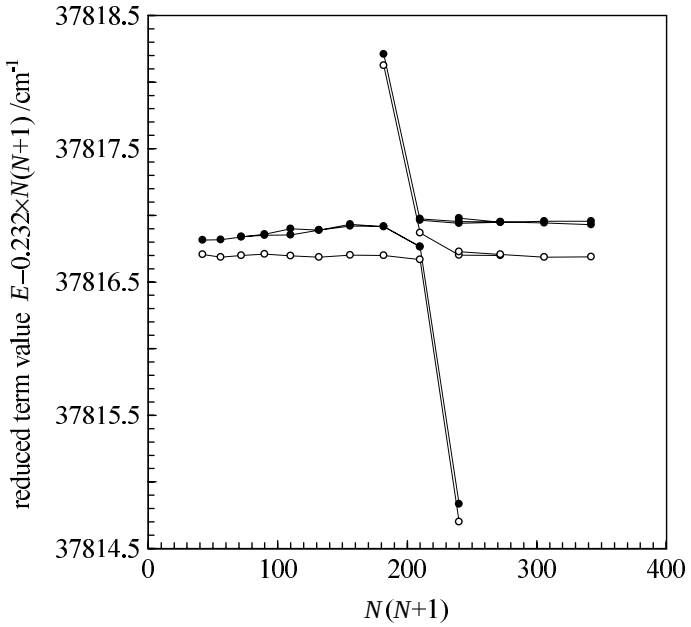

Figure 5. The very weak perturbation between the 10.88 $^2\Sigma^+$ state and an unknown core-non-penetrating state. (Open circles used for e-symmetry levels, solid circles for f-symmetry levels. Both e- and f-symmetry components of a $^2\Sigma^+$ state belong to + Kronig symmetry.) The perturbation affects both the e and f components equally and at the same N value. This shows that the core-non-penetrating states have negligible spin doubling (i.e. each ℓ, $\mathcal{L}$, N substate consists of two near degenerate $J = N \pm \frac{1}{2}$ spin components which belong to the same total parity, same Kronig symmetry, but opposite e/f symmetry). The numerous small doublings are not perturbations, they reflect small differences in term values calculated from observed rotational transitions terminating on the same final state.

that the two non-penetrating components undergo an avoided crossing right at the intersection with the $^2\Sigma^+$ state. A similar double perturbation is observed in the 11.86 $^2\Sigma^+$ state, shifted as expected to lower N values.

(*e*) *Perturbations in the 0.94* $^2\Delta$ *series*

Both + and − Kronig symmetry components of the 10.94 $^2\Delta$ state are perturbed at $N \approx 11$–12 (see figures 1 and 2). The two perturbers fall almost exactly on top of each other at low N, despite the fact that they have opposite Kronig symmetry hence must belong to different ℓ values. From the observed (not deperturbed) extra lines

$$\Delta T(8.5) = T_{\rm pert}(9) - T_{\rm pert}(8) = 2.96\ {\rm cm}^{-1} \qquad (3.9\,a)$$

$$= 2B^+[9 - \mathcal{L}], \qquad (3.9\,b)$$

and $B^+ \approx 0.234\ {\rm cm}^{-1}$, we obtain,

$$\mathcal{L}_{\rm exp} \approx 2.7,$$

which suggests that Δ^+ is perturbed by $h, \mathcal{L} = 3$ and Δ^- by $g, \mathcal{L} = 3$. These perturbations are quite strong and the $\Delta T(N + \frac{1}{2})$ values vary strongly with N. The behaviour of the 10.94 $^2\Delta^-$ state is regular outside of the perturbation region, therefore a simple two level deperturbation is possible. The observed deperturbed

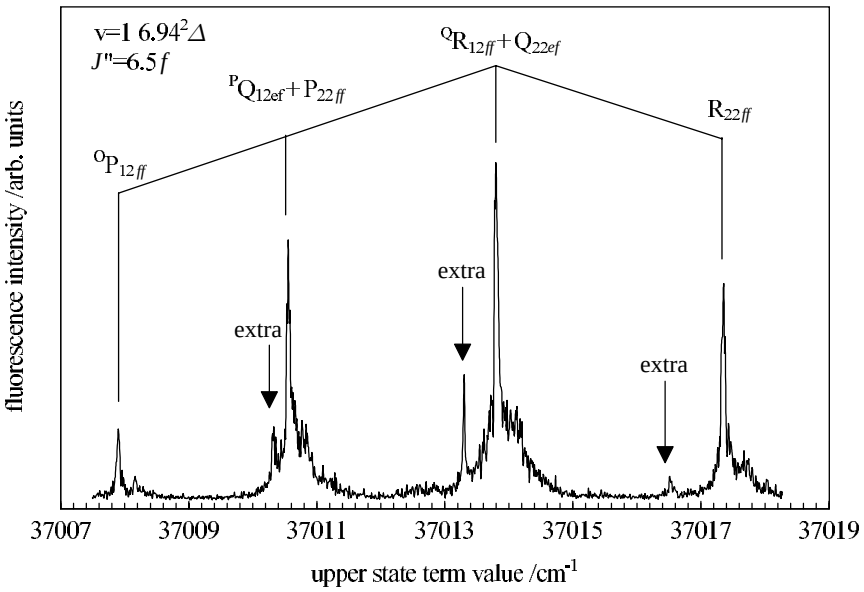

Figure 6. Weak extra lines near the $v^+ = 1$ 6.94 $^2\Delta$ state, assigned to an unknown core-non-penetrating perturber. These transitions originate from $J = 6.5f$ ($N = 7$) of $C\,^2\Pi_{3/2}$. The arrows mark the position of the core-non-penetrating perturbing state. The extra line near the P(7) ($^{P}Q_{12ef} + P_{22ff}$) main line actually perturbs the O(7) ($^{O}P_{12ff}$) main line, because of the $\Delta J = 0$ perturbation selection rule (see figure 7).

value, $\mathcal{L}_{\rm exp} \approx 3.3$, supports the above $\mathcal{L} = 3$ assignment. $\mathcal{L}_{\rm exp}$ appears to increase slightly with N. Our very crude analysis likely breaks down for such low N values (before the non-penetrating complexes have reached the case (d) limit) and for a core-penetrating state ($n^* = n + 0.94$) predicted to lie *within* rather than *just below* the n^* range of the g ($n^* = n + 1.09$ to 0.88) and h ($n^* = n + 1.05$ to 0.93) complexes.

The $v = 1$ 6.94 $^2\Delta$ state contains some information that may be relevant to the identity of the main (core-non-penetrating) perturber of the 10.88 $^2\Sigma^+$ state (because the perturber of $v = 1$ 6.94 $^2\Delta$ discussed here may be identical to the perturber of $v = 0$ 10.88 $^2\Sigma^+$). Figures 6 and 7 show a very weak perturbation, near $J = 5.5f$ in the $v = 1$ 6.94 $^2\Delta$ state. The perturber has an anomalously small $B_{\rm eff} \approx 0.20$ cm^{-1}, and is therefore a component of a non-penetrating complex. The perturbers, both e- and f-symmetry levels, are observed for all J between 5.5 and 10.5, but only the main $J = 5.5f$ level is detectably shifted, by only 0.028 cm^{-1}. However, the $\mathcal{L}_{\rm exp} \approx 1.25$ value derived from this assignment appears to be too small. This perturber of $v = 1$ 6.94 $^2\Delta$ probably also affects other members of the $v = 0$ and 1 manifolds of the 0.94 $^2\Delta$ series at J values below $J = 5.5f$ and $J = 6.5e$, which are the low-J limits of our OODR Rydberg spectra. (Note that the low-J limits mentioned in § 3 *a* apply to the intermediate $C\,^2\Pi$ state. These limits are the Rydberg levels that can be reached from $J = 6.5f$ of $C\,^2\Pi_{3/2}$.) Thus, except for $v = 1$ of 6.94 $^2\Delta$, we do not observe these perturbations. The $v = 1$ 6.94 $^2\Delta$ state is unique because it is strongly perturbed by the $v = 0$ 7.94 $^2\Delta$ state (intra-channel perturbation, see Murphy *et al.* (1995) and Herzberg & Jungen (1972)). As a result $v = 1$ 6.94 $^2\Delta$ is pushed to lower energy and the perturbation by the core-non-penetrating state is shifted to higher J values, well within the range observable in our OODR spectra.

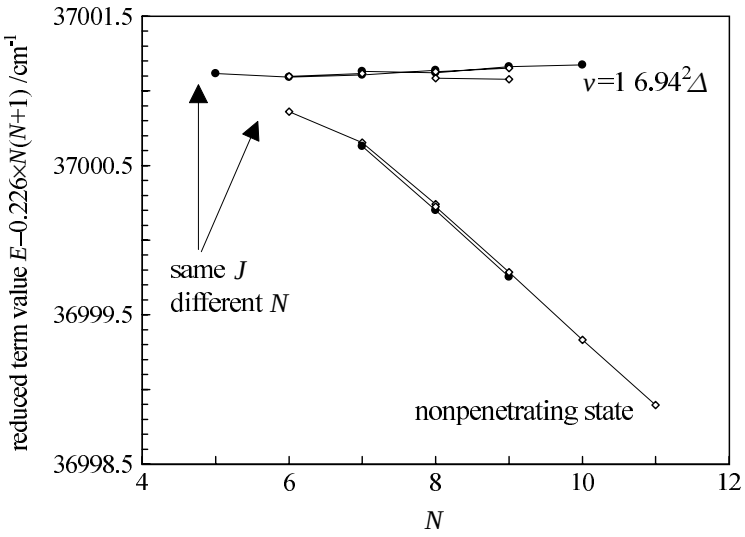

Figure 7. Plot of reduced term value versus N for the $v^+ = 1$ 6.94 $^2\Delta$ state and its unknown core-non-penetrating perturber. The term curves show curvature characteristic of a weak perturbation which culminates at a J value just below the lowest accessible ($J = 5.5f$ or $6.5e$) in our experiments via the $C^2\Pi_{3/2}$ intermediate state. Once again, an N plot makes it difficult to see the pattern of a $\Delta J = 0$, $\Delta N = 1$ perturbation.

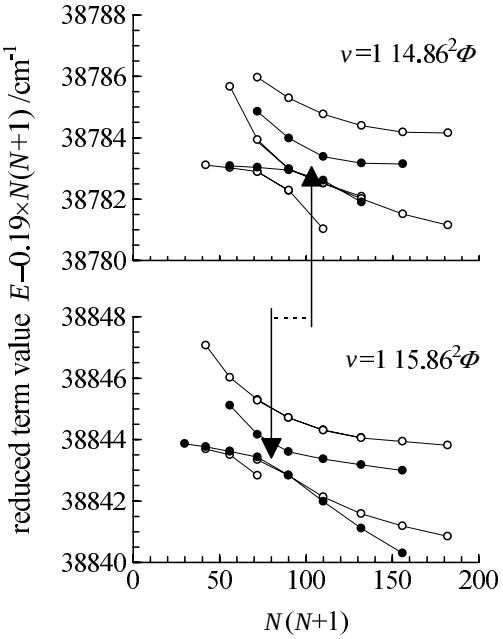

Figure 8. Plot of reduced term values versus $N(N+1)$ for $v^+ = 1$ members of the autoionizing 0.86 $^2\Phi$ series (open (filled) circles are $+(-)$ Kronig symmetry states). The $^2\Phi$ state is crossed from above by several non-penetrating states which shift toward lower N as n^* increases. Corresponding perturbations in the $^2\Phi^-$ component are indicated by arrows. The weaker lower-N perturbation in the $^2\Phi^+$ component is probably due to an $\ell = 6$ (i), $\mathcal{L} = 6$ perturber.

(f) *Perturbations in the* $v^+ = 1$ *0.86* $^2\Phi$ *series*

Figure 8 shows perturbations in the autoionizing $v^+ = 1$, 14.86 and 15.86 $^2\Phi$ states, obtained from spectra recorded with Dr Ma Hui at Tsinghua University (Ma *et al.*, unpublished work). These spectra also illustrate the expected shift of perturbations by non-penetrating states to lower N as n^* increases. In fact, the single weak perturbation in the − Kronig symmetry states (solid circles) is the same $\ell = 5$, $\mathcal{L} = 4$ (deperturbed $\mathcal{L}_{\rm exp} = 4.0$ and 3.9 for the $v^+ = 14.86$ $^2\Phi^-$ and $v^+ = 15.86$ $^2\Phi^-$ states, respectively) perturbation illustrated in the $v^+ = 0$ $^2\Phi$ states shown in figures 1–3. The $^2\Phi^+$ state (open circles) is perturbed by two core-non-penetrating states. The weaker perturbation (deperturbed $\mathcal{L}_{\rm exp} = 5.0$) is due to the $\ell = 5$, $\mathcal{L} = 5$ perturbation illustrated in figures 1–3. This perturbation is also observed in the $v^+ = 13.86$ $^2\Phi^+$ state and fragmentarily (one extra line and several small level shifts) in the $v^+ = 15.86$ $^2\Phi$ state (marked by $*$ in figure 8). The strong perturbation in both $v^+ = 14.86$ $^2\Phi^+$ and $v^+ = 15.86$ $^2\Phi^+$ is due to a state with lower $\mathcal{L}$ value. The onset of this perturbation is observed at high N in $v^+ = 10.86$ $^2\Phi^+$, 11.86 $^2\Phi^+$, and 12.86 $^2\Phi^+$ (see figures 1 and 3).

(g) n^**-scaling rules*

The core-penetrating and non-penetrating Rydberg states within each integer region of n^* form a pattern which exhibits characteristic n^*-scaling behaviours (Herzberg & Jungen 1972). For example, all rotationless energy spacings scale as n^{*-3},

$$E_{n^*+\delta/2} - E_{n^*-\delta/2} = \frac{2\mathcal{R}\delta}{n^{*3}}\left[1 + \frac{\delta^2}{2n^{*2}}\right]. \tag{3.10}$$

Rotational effects are included by noting that, in both case (b) and (d) limits, the effective rotational constant is the rotational constant of the ion core, B^+. However, in the case (d) limit, all of the core-non-penetrating states are arranged into same-(N, $\mathcal{L}$) clusters,

$$T^{(\rm d)}(N, \mathcal{L}) - B^+N(N+1) = B^+[\mathcal{L}(\mathcal{L}-1) - 2\mathcal{L}N]. \tag{3.11}$$

The energy spacings of the zero-order substates within each $N, \mathcal{L}$ cluster, which belong to different ℓ values, are independent of N and scale as

$$E_{n^*,\ell+1,N,\mathcal{L}} - E_{n^*,\ell,N,\mathcal{L}} = -2\mathcal{R}[\bar{\mu}_{\ell+1} - \bar{\mu}_\ell]/n^{*3}, \tag{3.12}$$

where $\bar{\mu}_\ell$ is the centre of gravity of the rotationless quantum defects for the Λ components of the ℓ complex. Equation (3.12) neglects off-diagonal $\Delta N = 0$, $\Delta\mathcal{L} \neq 0$ core–multipole interactions between members of different $\mathcal{L}$ clusters. This neglect is reasonable because the energy differences scale as

$$E_{N,\mathcal{L}} - E_{N,\mathcal{L}-1} = B^+[2(\mathcal{L}-1) - 2N], \tag{3.13}$$

and the off-diagonal matrix elements vary more slowly than linearly in N. Since all off-diagonal core-multipole matrix elements between members of different Rydberg series scale (Herzberg & Jungen 1972) as

$$\langle n_i^*|\boldsymbol{H}'|n_j^*\rangle \propto (n_i^* n_j^*)^{-3/2}, \tag{3.14a}$$

or, for $n_i^* \approx n_j^* \equiv n^*$,

$$\langle n_i^*|\boldsymbol{H}'|n_j^*\rangle \propto n^{*-3}. \tag{3.14b}$$

The ℓ mixing among the different ℓ components in each $N, \mathcal{L}$ cluster,

$$\theta_{ij} \equiv \frac{H'_{ij}}{\Delta E^{\circ}_{ij}}, \tag{3.15}$$

is n^* independent (and N independent), where θ is the mixing angle defined by ordinary non-degenerate perturbation theory! Of course, interactions that have so far been neglected will accidentally (at modest n^*) and systematically (at very high n^*) disrupt this n^*, N independence of the ℓ, ℓ' mixing coefficients among the non-penetrating Rydberg states. Foremost among the pattern destroying effects at modest n^* are the penetrating–non-penetrating perturbations. These perturbations also exhibit a characteristic n^*, N scaling. As long as the penetrating states follow case (b) (not too large N) and the non-penetrating states follow case (d) (not too small N), the N values of the $\Delta N = 0$ intersections between the rotational term curves move systematically to lower N as n^* increases. For the ith core-penetrating state near n with rotationless energy $E_{n-\mu_i}$,

$$T^{(\mathrm{b})}_{i,n}(N) = E_{n-\mu_i} + B^+ N(N+1), \tag{3.16}$$

and for the non-penetrating ℓ complex near n with rotationless energy $E_{n-\bar{\mu}_\ell}$,

$$T^{(\mathrm{b})}_{i,n}(N) - T^{(\mathrm{d})}_{n,\ell,\mathcal{L}}(N) = 0 = [E_{n-\mu_i} - E_{n-\bar{\mu}_\ell}] - B^+[\mathcal{L}(\mathcal{L}-1) - 2\mathcal{L}N], \tag{3.17}$$

$$E_{n-\mu_i} - E_{n-\bar{\mu}_\ell} = -2\mathcal{R}\frac{\mu_i - \bar{\mu}_\ell}{n^3}, \tag{3.18}$$

$$N_{\mathrm{cross}} = \frac{\mathcal{R}}{B^+} n^{-3} \frac{\mu_i - \bar{\mu}_\ell}{\mathcal{L}} + \tfrac{1}{2}(\mathcal{L} - 1). \tag{3.19}$$

Note that, when $(\mu_i - \bar{\mu}_\ell) > 0$ (the penetrating state lies below the non-penetrating complex), all of the non-penetrating perturbers have $\mathcal{L} > 0$ and N_{cross} moves systematically to lower N value as n^* increases until N_{cross} reaches its asymptotic value

$$N_{\mathrm{cross,asy}} = \tfrac{1}{2}(\mathcal{L} - 1). \tag{3.20}$$

However, for $(\mu_i - \bar{\mu}_\ell) < 0$, the non-penetrating perturbers have $\mathcal{L} < 0$ and N_{cross} also moves systematically to lower N values as n^* increases, however, above a critical n^* value the perturbations will vanish because they would occur at negative values of N.

This scaling of penetrating–non-penetrating perturbations toward low N as n^* increases also implies that $\Delta n \neq 0$ perturbations of a penetrating state by non-penetrating components of other n complexes will pile up at low N (see $12.86\ {}^2\Phi$ in figure 3). For example, consider the perturbation of the i, n-penetrating state by the $n+1$, ℓ, $\mathcal{L}$ non-penetrating state. The crossing N value is

$$N^{\Delta n=+1}_{\mathrm{cross}} = \frac{\mathcal{R}}{B^+} n^{-3} \frac{1 + \mu_i - \bar{\mu}_\ell}{\mathcal{L}} + \tfrac{1}{2}(\mathcal{L} - 1). \tag{3.21}$$

For example, if $B^+ = 0.234$, μ_i and $\bar{\mu}_i$ are both negligible with respect to one, and $\mathcal{L} = 5$, then

$$N^{\Delta n=+1}_{\mathrm{cross}} = 9.4 \times 10^4 n^{-3} + 2,$$

and, by $n = 20$, the next n $\mathcal{L} = 5$ crossing has shifted down to $N = 14$! This implies that the window for observing 'isolated' penetrating–non-penetrating perturbations closes for BaF well before $n = 20$. For a lighter molecule (e.g. one with $B^+ = 1\ \mathrm{cm}^{-1}$), these inter-$n$ perturbations begin to pile up at slightly lower n ($N^{\Delta n=+1}_{\mathrm{cross}} = 14$, for $\mathcal{L} = 5$, occurs at $n = 12$).

(h) Non-penetrating states detected above integer n^*

The core-penetrating states located just above integer n^* should be well situated to serve as perturbation detectors for components of core-non-penetrating complexes which have negative $\mathcal{L}$ values. Unfortunately, the situation is more complex just above integer n^*. There are several reasons for this, as follows. (i) The two core-penetrating states just above integer n^*, 0.04 $^2\Pi$ and 0.08 $^2\Sigma^+$, lie too close to integer n^*, and probably lie between the highest few components of the g and h complexes. As a result, the easiest to assign $\mathcal{L} = -\ell$ fastest upward going component of each ℓ complex either does not cross the 0.04 $^2\Pi$ and 0.08 $^2\Sigma^+$ states or is sampled at too low N to have reached the characteristic case (d) behaviour (diagnostic slope on a reduced term value versus N plot). (ii) The core-penetrating states have effective B values which are larger than B^+ and are weakly n^* dependent. The reason for the larger slopes is that the off-diagonal ℓ uncoupling matrix elements for low-Λ states, $\sim [\ell(\ell+1) - \Lambda(\Lambda \pm 1)]^{1/2}$, are larger than for high-Λ states. Thus the n^*, N scaling of the penetrating–non-penetrating level crossings is more complicated than the simple zero-order pattern described in § 3 *f*. (iii) The effective B values for the 'bright' 0.04 $^2\Pi$ and 0.08 $^2\Sigma^+$ states may be so similar to those for the 'dark' $\mathcal{L} = 0$ or $\mathcal{L} = 1$ non-penetrating components that the multipolar interaction is large enough to 'light up' an entire non-penetrating term curve (and distort its otherwise diagnostic rotational term curve). (iv) We do not have very complete spectroscopic information about the 0.04 $^2\Pi$ and 0.08 $^2\Sigma^+$ states in the optimum $n^* = 6$–14 region.

4. Conclusion

Several core-penetrating–non-penetrating perturbations are observed in the OODR spectra of BaF. One component is definitively assigned as the $\ell = 5$ (h), $\mathcal{L} = 5$ component. Examples of non-penetrating states with $\mathcal{L}_{\rm exp} = 1$–5 have been observed. Core-penetrating series situated just above and below integer n^* are ideal detectors of non-penetrating states via perturbations. Of these, the easiest to detect and assign are those with highest $|\mathcal{L}|$ value, which correspond to the most rapidly downward ($\mathcal{L} > 0$) or upward ($\mathcal{L} < 0$) going components on a reduced term value plot. Assignments of other smaller-$|\mathcal{L}|$ perturbers are less reliable and will require further analysis.

The naively expected n^*, N scaling of the level patterns is discussed. Each penetrating–non-penetrating perturbation is expected to be replicated, shifted to lower N-value, as one goes from the n^* complex to the $n^* + 1$ complex. This pattern of replicated perturbations has been observed (figures 3 and 4), but will be more fully documented in a subsequent publication.

Before attempting a global multi-state fit to all of the recorded BaF spectral data, from which BaF^+ multipole moments and polarizabilities would be obtained, it is necessary to refine the single state assignments (Jakubek & Field 1996) and determine sets of state–by–state molecular constants by local deperturbations (Jakubek & Field 1998). Above all, it is essential to know how the ten well known and spectroscopically 'bright' s∼p∼d∼f core-penetrating $^2\Lambda$ states (Jakubek & Field 1994) sample the underlying zero-order pattern of core-non-penetrating states via perturbations: which ℓ are detectable; what is the case (d) rotational pattern (clusters of same-$N, \mathcal{L}$ states; $\mathcal{L}$-diagnostic slopes on reduced term value versus N plots; n^*-independent ℓ mixing within $N, \mathcal{L}$ clusters); and what causes the naive zero-order

patterns to break down? The present paper is the first small step toward a global model for the non-penetrating Rydberg states of BaF.

This research was supported by a grant from the National Science Foundation (CHE91–20339). We thank Dr Christian Jungen for helpful suggestions and Dr Ma Hui for his hospitality at Tsinghua University where he and Z.J.J. recorded many higher-n^* BaF spectra. Z.J.J. is grateful to the Fulbright Foundation for a Junior Fulbright Scholarship and to the MIT Chemistry Department for a Lester Wolfe Fellowship.

References

Alexander, M. H. & 28 others 1988 A nomenclature for Λ-doublet levels in rotating linear molecules. *J. Chem. Phys.* **89**, 1749–1753.

Berg, J. M., Murphy, J. E., Harris, N. A. & Field, R. W. 1993 Observation and analysis of core-penetrating Rydberg states of calcium monofluoride. *Phys. Rev.* A **48**, 3012–3029.

Dill, D. & Jungen, Ch. 1980 *J. Phys. Chem.* **84**, 2116–2122.

Dressler, K., Jungen, Ch. & Miescher, E. 1981 *J. Phys.* B **14**, L701–L704.

Effantin, C., Bernard, A., d'Incan, J., Wannous, G., Vergès, J. & Barrow, R. F. 1990 *Mol. Phys.* **70**, 735–745.

Eyler, E. E. & Pipkin, F. M. 1986 *Phys. Rev.* A **34**, 2881–2888.

Field, R. W. & Gittins, C. M. 1997 Realistic representation of the induced electric dipole moment of a polarizable ligand: the missing factor in the Rittner Polarizability. *J. Chem. Phys.* **106**. (In the press.)

Fujii, A. & Morita, N. 1995 *J. Chem. Phys.* **103**, 6029–6039.

Gerstenkorn, S. & Luc, P. 1979 Atlas du spectre d'absorption de la molécule d'iode (CNRS, Paris, 1978); *Rev. Phys. Appl.* **14**, 791–794.

Gittins, C. M., Harris, N. A., Field, R. W., Vergès, J., Effantin, C., Bernard, A., d'Incan, J., Ernst, W. E., Bündgen, P. & Engels, B. 1993 Analysis and deperturbation of the $C^2\Pi$ and $D^2\Sigma^+$ states of CaF. *J. Mol. Spectrosc.* **161**, 303–311.

Harris, N. A. & Field, R. W. 1993 The core-penetrating Rydberg series of the CaF molecule: at the borderline between valence and Rydberg states. *J. Chem. Phys.* **98**, 2642–2646.

Harris, N. A. & Jungen, Ch. 1993 Rydberg states of calcium fluoride. *Phys. Rev. Lett.* **70**, 2549–2552.

Herzberg, G. & Jungen, Ch. 1972 *J. Mol. Spectrosc.* **41**, 425–486.

Herzberg, G. & Jungen, Ch. 1982 *J. Chem. Phys.* **77**, 5876–5884.

Huber, K. P., Jungen, Ch., Yoshino, K., Ito, K. & Stark, G. 1994 The *f* Rydberg series in the absorption spectrum of N_2. *J. Chem. Phys.* **100**, 7957–7972.

Jakubek, Z. J. & Field, R. W. 1994 The core-penetrating Rydberg series of BaF: s∼p∼d∼f super-complexes. *Phys. Rev. Lett.* **72**, 2167–2170.

Jakubek, Z. & Field, R. W. 1996 Core-penetrating Rydberg series of BaF: new electronic states in the $n^* \approx 4$ region. *J. Mol. Spectrosc.* **179**, 99–124.

Jakubek, Z. J. & Field, R. W. 1998 Core-penetrating Rydberg series of BaF: single state fits of new electronic states in the $4.4 < n^* < 14.3$ region. *J. Mol. Spectrosc.* (Submitted.)

Jakubek, Z. J., Harris, N. A., Field, R. W., Gardner, J. A. & Murad, E. 1994 The ionization potentials of CaF and BaF. *J. Chem. Phys.* **100**, 622–627.

Jungen, Ch. & Miescher, E. 1969 *Can. J. Phys.* **47**, 1769–1787.

Komatsu, M., Ebata, T., Maeyama, T. & Mikami, N. 1995 Rotational structure and dissociation of the Rydberg states of CO investigated by ion–dip spectroscopy. *J. Chem. Phys.* **103**, 2420–2435.

Lefebvre-Brion, H. & Field, R. W. 1986 *Perturbations in the spectra of diatomic molecules*, p. 465. London: Academic.

Li, J., Liu, Y., Moss, D. B., Clevenger, J., Gittins, C., Harris, N. & Field, R. W. 1998 Double resonance spectroscopic studies of $^2\Sigma^+$ Rydberg states of CaCl. (In preparation.)

McCormack, E. F., Pratt, S. T., Dehmer, J. L. & Dehmer, P. M. 1990 Double resonance spectroscopy of autoionizing states of N_2 near the ionization threshold. *Phys. Rev.* A **42**, 5445–5451.

Mulliken, R. S. 1964 In a characteristically obscure but profound quotation: 'Ontology recapitulates phylogeny', Robert Mulliken borrows from biology to explain spectroscopy. *J. Am. Chem. Soc.* **86**, 3183–3197.

Murphy, J. E., Berg, J. M., Merer, A. J., Harris, N. & Field, R. W. 1990 Rydberg states of calcium monofluoride. *Phys. Rev. Lett.* **65**, 1861–1864.

Murphy, J. E., Friedman-Hill, E. & Field, R. W. 1995 A multichannel quantum defect fit to the $n^* = 6$–8 core-penetrating s∼p∼d supercomplexes of CaF. *J. Chem. Phys.* **103**, 6459–6466.

Rice, S. F., Martin, H. & Field, R. W. 1985 The electronic structure of the calcium halides. A ligand field approach. *J. Chem. Phys.* **82**, 5023–5034.

Ross, S. 1991 An MQDT primer. In *Half collision resonance phenomena in molecules*, AIP Conference Proceedings 225, Proceedings of the Escuela Latinamericana de Fśica, Caracus, Venezuela, 1990 (ed. M. García-Sucre, G. Raseev & S. C. Ross), pp. 73–110. New York: AIP.

Sturrus, W. G., Hessels, H. A., Arcuni, P. W. & Lundeen, S. R. 1988 *Phys. Rev.* A **38**, 135–151.

Watson, J. K. G. 1994 *Mol. Phys.* **81**, 277–289.